ELSEVIER

Polymer 42 (2001) 6929–6943

polymer

www.elsevier.nl/locate/polymer

Gas and vapor sorption and diffusion in poly(ethylene terephthalate)

G.E. Serad[a], B.D. Freeman[a,*], M.E. Stewart[b,1], A.J. Hill[c,d]

[a]*Department of Chemical Engineering, North Carolina State University, Raleigh, NC 27695-7905, USA*
[b]*Eastman Chemical Company, P.O. Box 1972, Kingsport, TN 37662-5150, USA*
[c]*CSIRO Manufacturing Science and Technology, Private Bag 33, Clayton South, Vic., MDC 3169, Australia*
[d]*Department of Chemistry, Monash University, Clayton, Vic. 3168, Australia*

Received 10 July 2000; received in revised form 1 February 2001; accepted 5 February 2001

Abstract

Equilibrium sorption of *n*-butane and acetaldehyde in melt-processed poly(ethylene terephthalate) (PET) microtomed flakes is reported. The *n*-butane sorption isotherm at 35°C is well described by the dual-mode model with the following parameters: $k_D = 0.017$ cm^3 (STP)/(cm^3 amorphous polymer cmHg), $C'_H = 1.3$ cm^3 (STP) (cm^3 amorphous polymer) and $b = 0.029$ cmHg^{-1}. Acetaldehyde isotherms at 35 and 45°C may be described by the Flory–Huggins sorption model, suggesting that penetrant uptake in the non-equilibrium excess volume associated with the glassy polymer made a negligible contribution to the overall sorption level at the conditions of this study. The heat of sorption was essentially equal to the enthalpy of condensation of pure acetaldehyde. At 45°C and acetaldehyde pressures at or above 40.0 cmHg, acetaldehyde triggers significant crystallization of PET (up to 37 wt%) with increasing concentration. Subsequent sorption experiments at very low penetrant activity reveal solubility coefficients that are markedly higher in the penetrant-crystallized sample than in the initially highly amorphous sample. This result suggests the acetaldehyde-induced formation of microvoids (which act as highly efficient penetrant sorption sites) in the polymer sample. Based on these and literature data, the logarithm of infinite dilution penetrant solubility in amorphous regions of PET was well-correlated with penetrant condensability as characterized by T_c, penetrant critical temperature, or by $(T_c/T)^2$, where T is the experiment temperature. Infinite dilution, amorphous phase penetrant diffusion coefficients in PET decreased according to a power law relation with increasing penetrant critical volume.

Keywords: Sorption; Diffusion; *n*-Butane

1. Introduction

Poly(ethylene terephthalate) (PET) is a widely used barrier packaging material [1]. While sorption and transport of gases such as oxygen and carbon dioxide are important considerations in designing barrier packaging, the sorption of organic flavor molecules, such as *d*-limonene, into package walls is important in determining flavor scalping and, in refill applications, flavor carryover and contamination [2]. The migration of such components depends on both penetrant solubility and diffusivity. However, sorption and transport data for flavor molecules or other large organic penetrants in barrier packaging are not readily available.

In this study, the solubilities of *n*-butane and acetaldehyde in thin, microtomed PET flakes were determined as a function of pressure. These results are complemented by differential scanning calorimetry, densitometry, wide angle X-ray diffraction (WAXD) spectroscopy, positron annihilation lifetime spectroscopy, ^{13}C solid state nuclear magnetic resonance cross polarization magic angle spinning spectroscopy, and gel permeation chromatography characterization of the polymer. Additionally, results of a literature survey of solubility and diffusivity data for penetrants in PET are presented, and general correlations of infinite dilution penetrant solubility with critical temperature and infinite dilution penetrant diffusivity with critical volume are provided.

2. Experimental

2.1. Sample preparation

PET (Eastapak™ Polymer 9663) pellets were kindly supplied by Eastman Chemical Company (Kingsport, TN). One-eighth inch thick tensile bars were molded from the pellets using a Toyo 90 injection molder (Toyo Machinery and Metal, Singapore). A chilled mold at −3°C was used to

* Corresponding author. Tel.: +1-919-515-2460; fax: +1-919-515-3465.
E-mail address: benny_freeman@ncsu.edu (B.D. Freeman).
[1] Tel.: +1-423-229-2582; fax: +1-423-229-6183.

0032-3861/01/$ - see front matter
PII: S0032-3861(01)00120-3

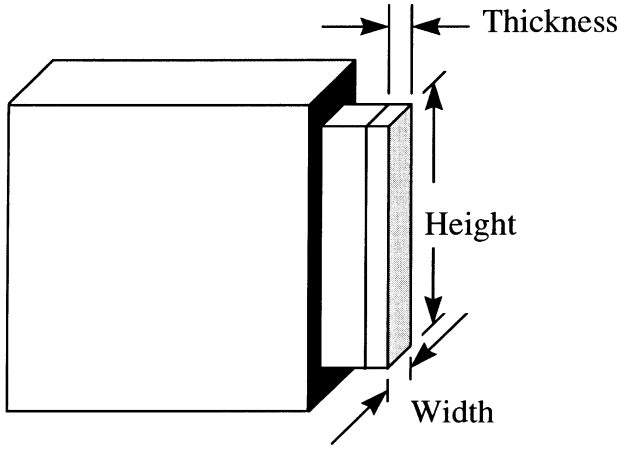

Fig. 1. PET Tensile bar prepared for microtoming. The black area is the original cross section of the tensile bar, and the gray area was used to prepare microtomed flakes. The width, height, and thickness dimensions of the microtomed flakes were 1mm, 9 mm, and 2 μm, respectively.

rapidly quench the molten polymer from the injection temperature, 281°C, to obtain highly amorphous samples.

Thin, uniform sheets (or flakes) were microtomed from the tensile bars. Two samples for microtoming were cut from the center of each tensile bar. The blocks were first trimmed using a Reichert (Buffalo, NY) Ultracut S microtome and a glass microtome knife. A schematic of a trimmed sample is shown in Fig. 1.

PET flakes were microtomed from the trimmed sample blocks using a Reichert Ultracut S microtome equipped with a Reichert FCS cryo-system. The microtomed flakes were 2 μm in thickness, 1 mm in width, and 9 mm long. The microtome knives were Diatome (Fort Washington, PA) 45° cryo-histo diamond knives with 4 mm blades. The microtome was operated at −80°C to minimize any changes in the polymer structure due to the microtoming process. A clearance angle of 2°, a cutting speed of 1 mm/s, and the maximum return speed setting were used. Approximately 11 000 microtomed flakes (~340 mg) were collected. Two Diatome cryo-histo microtome knives were required. Each knife developed nicks and was replaced after about 6000 flakes were microtomed. To obtain samples with the most uniform thickness possible, the microtomed flakes were collected, in the order in which they were generated, in 18 separate vials, each containing 12–20 mg of polymer.

2.2. Gravimetric sorption

Gravimetric sorption experiments were performed using both a McBain spring balance [3] system and a Cahn RG Electrobalance (Bellflower, CA). The McBain spring system consists of a water-jacketed glass chamber serviced by a vacuum pump for polymer degassing and penetrant removal. The chamber temperature was controlled by a water bath. Approximately 30.0 mg of PET microtomed flakes were loaded into a cylindrical quartz pan suspended from a sensitive helical quartz spring in the chamber. The spring (model 4501.6) and sample pan (model 4505.2-2) were supplied by Ruska Industries, Inc. (Houston, TX). The spring extension was 1 mm for every 0.152 mg of load.

Before beginning sorption experiments, the sample was exposed to vacuum until there was no further spring displacement to remove previously sorbed air gases from the polymer. Then the sample was exposed to penetrant at a fixed pressure, and the spring position relative to a fixed reference rod hanging in the chamber was recorded using a Cohu (San Diego, CA) 4910 CCD camera [4]. The camera was interfaced to an Apple Macintosh 7600/132 computer via a Scion Corporation LG-3 frame grabber card (Frederick, MD). Image, a software package from the National Institutes of Health (NIH), was used to store and process data from the camera. Using this apparatus, spring position was recorded as a function of time using a special Image macro written for sorption data collection [4]. The spring position data were converted to mass uptake data using the spring constant.

A Cahn model RG electrobalance serviced by a vacuum system was also used to collect *n*-butane gravimetric sorption data. The balance was housed in an insulated box equipped with an air bath temperature regulation system. A quartz hemispherical pan supplied by Ruska Industries, was filled with 48.3 mg of PET microtomed flakes and placed on the balance. After degassing under vacuum, the sample was exposed to penetrant at fixed pressure, and a Fisher (Pittsburgh, PA) Recordall Series 5000 chart recorder monitored sample mass as a function of time.

2.3. Nuclear magnetic resonance spectroscopy characterization

The microtomed flakes and an unmicrotomed control were characterized using ^{13}C solid state cross polarization magic angle spinning (CPMAS) NMR spectroscopy. Data were obtained at ambient temperature using a Bruker MSL-400 NMR spectrometer (Billerica, MA) with a nominal operating frequency for carbons at 100.61 MHz. All ^{13}C chemical shifts were referenced to the resonance of tetramethylsilane. Each spectrum in the carbon spin lattice relaxation time (T_1) measurement is the average of 3600 scans, with a repetition time of 5 s, and at variable delays ranging from 1 ms to 80 s.

2.4. Gel permeation chromatography and inherent viscosity

A gel permeation chromatograph (GPC) was used to determine number and weight average molecular weights of the tensile bar samples at 25°C and atmospheric pressure. Polymer Labs (Amherst, MA) 5 μm Mixed-C PL gel columns were used with a carrier solvent of 5/95 (v/v) hexafluoroisopropanol/methylene chloride containing 0.1 g of tetraethylammoniumbromide per 100 ml of solvent. The detector was a Perkin–Elmer (Norwalk, Connecticut) LC235 UV absorbance detector. The original solution

injected into the column was an azeotropic hexafluoroisopropanol/methylene chloride solution containing 0.4 mg of PET per ml of solution.

The inherent viscosity of the tensile bar samples was determined at 25°C and atmospheric pressure by measuring the PET solution viscosity and using an established correlation to relate solution viscosity to inherent viscosity. A Schott AVS 500 viscometer (Yonkers, NY) was used to determine solution viscosity. The solvent was a 60/40 (w/w) phenol/tetrachloroethane mixture. The polymer concentration was 0.5 wt%.

2.5. Thermal and physical characterization

A density gradient column containing an aqueous solution of lithium bromide was prepared with densities ranging from 1.30 to 1.35 g/cm^3. This column was used to determine the density of two tensile bar samples. Each sample was tested twice. The weight percent crystallinity was determined based on the sample densities and published densities for wholly amorphous and completely crystalline PET [5]. A Scintag PAD-S X-ray diffractometer (Cupertino, CA) with a Cu Kα ($\lambda = 1.54$ Å) X-ray source was used to characterize crystallinity in both the PET tensile bar and microtomed flakes.

Thermal transitions were determined by differential scanning calorimetry (DSC). A tensile bar sample taken from the center core of the bar and a sample of microtomed flakes (prior to penetrant exposure) were analyzed using a TA Instruments 2920 differential scanning calorimeter (New Castle, DE). To minimize the effects of absorbed water, specimens were dried in a vacuum oven at room temperature for 1 week prior to the DSC measurements. First and second scan thermograms were recorded at a heating rate of 20°C/min. From the first heating thermogram, cold crystallization and melting temperatures were determined. The areas under the cold crystallization and melting peaks were used to calculate the wt% crystallinity of the tensile bar as described previously [6]. The second scan thermogram was used to determine the glass transition temperature.

2.6. Positron annihilation lifetime spectroscopy

Positron annihilation lifetime spectroscopy (PALS) was used to characterize the amount of accessible free volume in various polymer samples. Measurements were made in air at room temperature (22.5 ± 1°C) using an automated EG and G Ortec fast–fast coincidence system. The timing resolution of the system was 275 ps determined using the prompt curve from a ^{60}Co source with the energy windows set to ^{22}Na events. The polymer films were stacked up to a total thickness of 1.5 mm when possible on either side of the 30 μCi ^{22}Na–Ti foil source. Five spectra for each sample were collected over a period of 8 h, and the results reported are the mean values for these spectra. The spectra were modeled as the sum of three decaying exponentials using the computer program PFPOSFIT [7]. The shortest lifetime was fixed at 125 ps characteristic of paraPositronium self annihilation. No source correction was used in the analysis based on a fit for pure Al standards of 169 ± 2 ps, 99.3 ± 0.3%; 820 ps, 0.7%. Only the orthoPositronium (oPs) components (the longest lifetime, τ_3 and its intensity I_3) are reported as it is the oPs component that is related to annihilations in free volume cavities of the polymer matrix [8].

3. Results and discussion

3.1. Polymer characterization

The average molecular weight of the PET tensile bars determined by GPC was: $M_n = 13\,000 \pm 1200$, $M_w = 41\,000 \pm 800$, and $M_z = 66\,500 \pm 500$ g/mol. The inherent viscosity was 0.672 ± 0.011 dl/g, which is also indicative of high molecular weight polymer. The uncertainties in inherent viscosity, GPC measurements and in subsequent polymer characterization results are based on the mean and standard deviations of multiple sample analyses.

A ^{13}C solid state CPMAS NMR spectrum for the microtomed sample is presented in Fig. 2. The four principal carbon atom assignments for the PET repeat unit are indicated. The spectral line widths and relative intensities of the methylene and carbonyl groups are sensitive to the level of crystallinity in PET [9]. Therefore, a comparison of the CPMAS spectrum of the microtomed flakes with that of unmicrotomed samples provides a qualitative indication of the extent of crystallinity or constraints developed in the sample due to microtoming. Fig. 3 presents CPMAS NMR spectra of microtomed flakes and extruded, undrawn PET films (Eastapak™ Polymer 9921W) that were annealed, as described by Fischer and Fakirov [10], to develop the levels of crystallinity indicated in the figure. Peak widths of the microtomed flakes and unmicrotomed amorphous film are

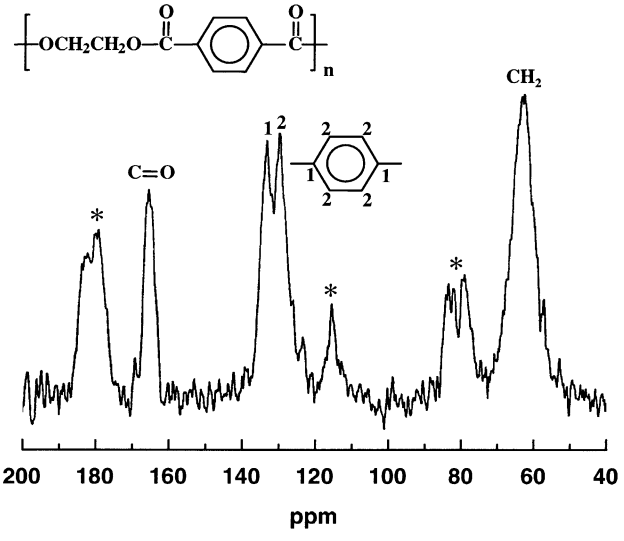

Fig. 2. ^{13}C Solid state CPMAS NMR spectrum of PET samples. * Spinning side bands.

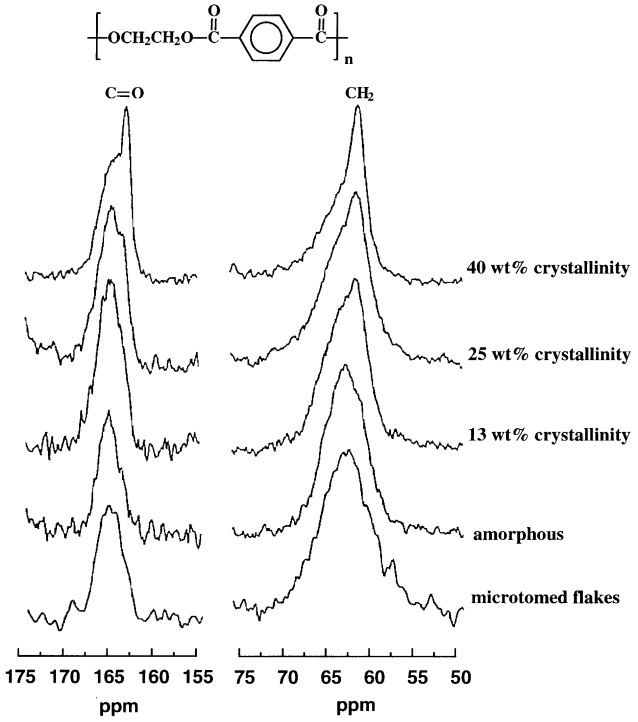

Fig. 3. ^{13}C Solid State CPMAS NMR spectra of microtomed flakes, amorphous extruded film, and films annealed to develop varying levels of crystallinity.

essentially the same. However, the annealed, semicrystalline films exhibit a decrease in the CH_2 peak width and the development of a rather sharp peak in the carbonyl region of the spectrum. These results indicate a biphasic structure in the annealed films consisting of relatively mobile amorphous regions and rigid, rather immobile crystalline regions. Based on these results, the microtomed flakes are largely amorphous, consistent with the highly amorphous character of the parent tensile bars.

The carbon spin lattice relaxation time, T_1, characterizes local segmental mobility in the principal PET carbons [9]. Table 1 contains T_1 values determined for microtomed flakes and for a 127 μm extruded film of the same composition as the pellets used for the injection molding of the tensile bars (Eastapak™ Polymer 9663). Based on its density, the extruded film had 5.8 wt% crystallinity. Within the uncertainty of the measurements, the T_1 values for the

Table 1
Carbon spin lattice relaxation times, T_1, from ^{13}C solid state CPMAS NMR analysis of PET film and microtomed flakes

ppm	T_1 127 μm film (s)	T_1 microtomed flakes (s)
163	64.1 ± 2.8	68.5 ± 4.1
131	51.7 ± 2.6	57.7 ± 4.3
129	39.4 ± 2.3	33.4 ± 8.2
60	[a]36.8 ± 7.1	[a]41 ± 8.8

[a] Values obtained based on single relaxation although multiple relaxations were evident.

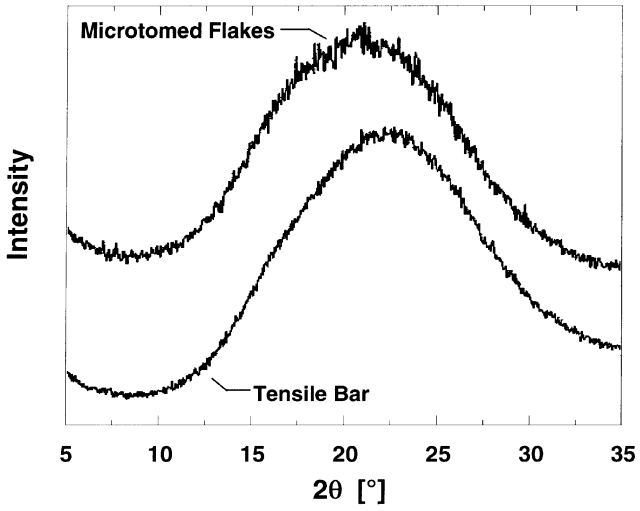

Fig. 4. Wide angle X-ray diffraction spectra of microtomed flakes and the parent tensile bar. The microtomed sample spectrum has been displaced vertically for easier viewing.

microtomed flakes and the film are the same, confirming that the microtomed flakes have molecular-level mobility, as probed by this experiment, consistent with that of thick extruded films.

The PET tensile bar density was 1.3391 ± 0.0006 g/cm^3. This corresponds to a wt% crystallinity of 7.1 ± 0.52%, or a vol.% crystallinity of 6.5 ± 0.48% based on an amorphous density, ρ_a, of 1.331 g/cm^3 and a crystalline density, ρ_c, of 1.455 g/cm^3 [5]. The density of microtomed flakes could not be determined by this method. Their high surface to volume ratio and tightly curled shape trapped air bubbles on the flakes. As a result, the flakes floated to the top of the density gradient column, thereby compromising a direct measurement of the density. Wide-angle X-ray diffraction spectra of both the tensile bars and microtomed flakes are presented in Fig. 4. These spectra contain only a broad amorphous halo and have essentially the same shape. The lack of discernible crystalline peaks indicates crystallinity levels of less than 10%, consistent with the density result.

First and second scan DSC thermograms for both the tensile bars and microtomed flakes are presented in Fig. 5. The tensile bars exhibited a glass/rubber transition, T_g, at 79°C, a cold crystallization exotherm, T_c, centered at 158°C, and a melting point, T_m, centered at 248°C. The microtomed flakes have a T_g at 78°C, a T_c at 137°C, and a T_m at 249°C. The transition temperatures, with the exception of T_c, are the same for both samples within the precision of the experiments, and are in excellent agreement with previously published values of T_g (81°C) and T_m (250–265°C) [11]. The cold crystallization peak was at a lower temperature in the microtomed sample, suggesting more facile crystal formation in these samples. However, the source of this difference is not well-understood. The weight percent crystalllinty of both samples was calculated by subtracting the enthalpy of cold crystallization from the enthalpy of

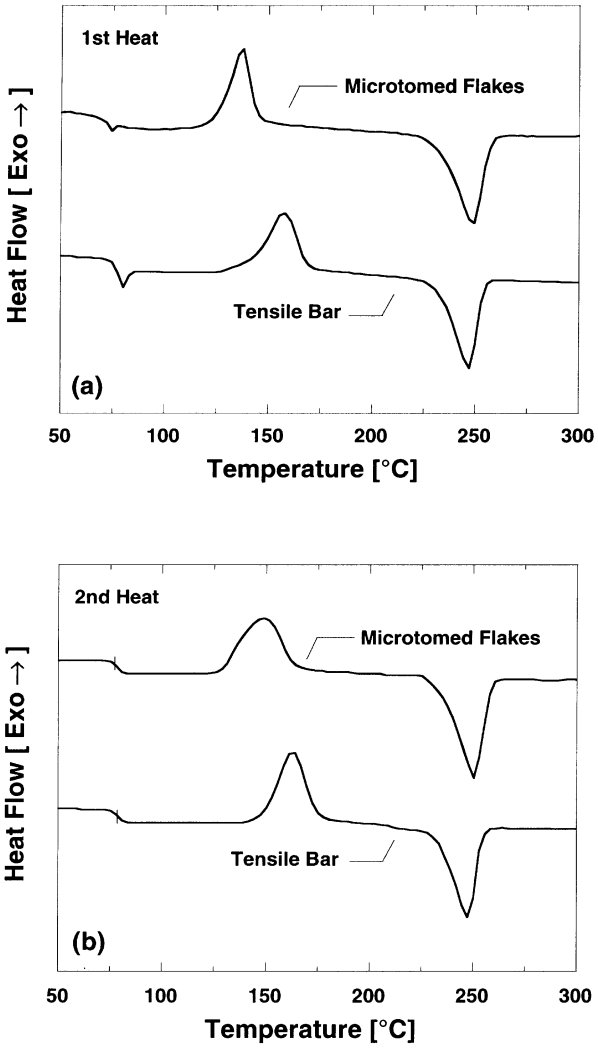

Fig. 5. Differential scanning calorimetry thermograms of PET microtomed flakes and tensile bar. (a) First heat, (b) second heat.

melting, and dividing by the heat of fusion of PET (29 cal/g) [12]. The wt% crystallinity for the microtomed flakes and the tensile bars was 5.5 and 0.3%, respectively.

The crystallinity level in the tensile bars determined by densitometry is very close to the value obtained by DSC for the microtomed flakes and is consistent with the X-ray diffraction and CPMAS NMR results for the tensile bars and flakes. Thus, if there is a change in the amount of crystallinity due to microtoming, it is near the resolution level of the techniques used in this study. Therefore, we use a value of 5.5 wt% for the crystallinity in the microtomed samples in subsequent estimations of amorphous phase solubility.

Density provides a measure of static free volume related to chain packing, but not dynamic, or sub-T_g mobility-related, free volume. Both types of free volume influence penetrant diffusion in polymers [8,13] and can be characterized by PALS. Dynamic and static free volume cavity size and the relative concentration of free volume cavities

Table 2
Positron annihilation lifetime spectroscopy results for PET samples prepared from microtomed flakes, a tensile bar, and an extruded, undrawn film

Sample	$\tau_3 \pm 0.03$ (ns)	$I_3 \pm 0.3$ (%)
Microtomed flakes	1.62	14.32[a]
Tensile bar	1.65	22.02
127 μm Extruded film	1.63	22.33

[a] This value reflects poor packing of the sample around the source, not a difference in free volume concentration.

accessible to *ortho*-positronium (*o*Ps) are probed by PALS [19]. τ_3, the average lifetime of *o*Ps in the polymer matrix, is a measure of the mean size of the cavity in which *o*Ps localizes in the polymer. I_3, the relative number of *o*PS annihilations, is a measure of the relative concentration of free volume cavities. The τ_3 and I_3 values for the PET tensile bars and microtomed flakes are recorded in Table 2. The PALS parameter values for the 127 μm extruded film, for which carbon spin lattice relaxation time were presented in Table 1, are included in Table 2 for comparison. Within experimental error, the PALS lifetime parameter is the same for all three samples, indicating that the average free volume element size probed by PALS is not sensitive to differences in the processing history of these samples. The I_3 parameter values for the tensile bars and extruded film are the same. The I_3 value of the microtomed flakes is significantly lower than that of the other samples. This is an artifact related to poor packing of the microtomed samples around the PALS source and does not indicate a difference in the concentration of free volume elements in the microtomed sample relative to the other samples. Based on these composite results, the cryomicrotoming process has not induced measurable changes in crystallinity, polymer morphology, or chain packing in the solid state.

3.2. Equilibrium n-butane uptake

The effect of *n*-butane pressure on the concentration of *n*-butane sorbed in the amorphous phase of the PET microtomed flakes is presented in Fig. 6. The penetrant concentration in the amorphous phase, C_a, is calculated from the total concentration of penetrant sorbed in the polymer, C, using the following relation [5,14–18]:

$$C = C_a \Phi_a, \tag{1}$$

where Φ_a is the polymer amorphous volume fraction.

The isotherm is concave to the pressure axis and is well described by the dual mode sorption model, which is typically used to model sorption of gases and vapors in glassy polymers [19]. This model assumes that penetrant sorption occurs in the equilibrium densified polymer matrix (so-called Henry's law sites) and in the nonequilibrium excess volume in the glassy polymer (so-called Langmuir sites). The model is expressed analytically as the algebraic sum

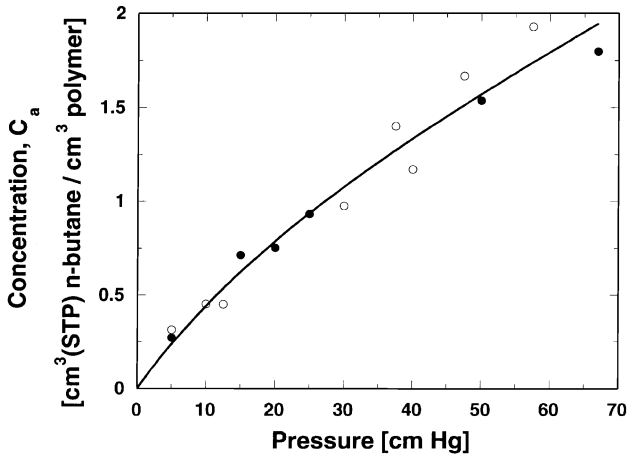

Fig. 6. *n*-Butane sorption isotherm in PET at 35°C. The saturation vapor pressure of *n*-butane at 35°C is 245.5 cmHg[26]. (●) Data obtained using McBain spring balance, (○) Data obtained using Cahn electrobalance. The concentration data are reported on an amorphous basis using Eq. (1) and an amorphous volume fraction of 0.95.

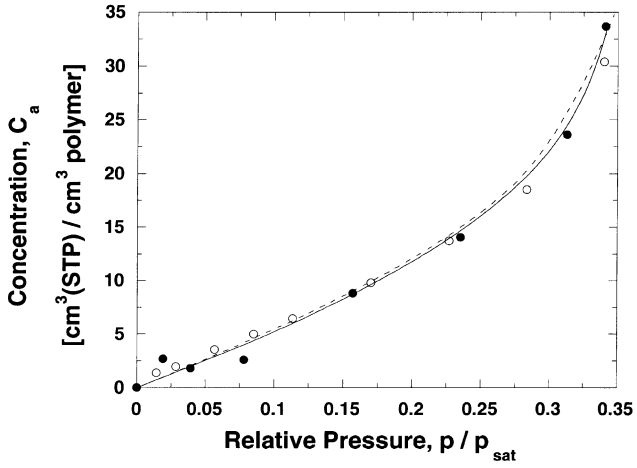

Fig. 7. Acetaldehyde concentration in amorphous regions of PET, C_a, at 35 and 45°C as a function of relative pressure. (●) 35°C, p_{sat} = 127.6 cm Hg[26], (○) 45°C, p_{sat} = 176.4 cm Hg[26]. The solid and dashed lines represent the best fit of the Flory–Huggins sorption model to the data at 35 and 45°C, respectively, with a concentration-dependent interaction parameter. All of these data were obtained using the McBain spring balance.

of the penetrant concentration in each mode [19]

$$C_a = k_D p + C'_H \frac{bp}{1 + bp}, \tag{2}$$

where p is pressure, k_D is the Henry's law coefficient, C'_H is the Langmuir capacity parameter, and b is the Langmuir affinity parameter. The solid curve in Fig. 6 is a least-squares fit of Eq. (2) to the sorption data. The dual-mode parameters are: $k_D = 0.017 \pm 0.003$ cm^3 (STP)/(cm^3 amorphous polymer cmHg), $C'_H = 1.3 \pm 0.2$ cm^3 (STP)/cm^3 amorphous polymer, and $b = 0.029 \pm 0.006$ cmHg^{-1}.

The gravimetric sorption experiments provide kinetics of penetrant uptake as well as equilibrium uptake. In samples of uniform, well-characterized thickness, the kinetic data may be used to determine penetrant diffusion coefficients. However, our microtomed flakes were curled, and an analysis of the kinetic data suggested that the surface area was not entirely accessible to penetrant. This factor complicates a rigorous determination of penetrant diffusion coefficients. As a result, only equilibrium penetrant uptake data are reported. A more complete analysis of the kinetic data obtained in this study is available elsewhere [20].

3.3. Equilibrium acetaldehyde uptake

Fig. 7 presents acetaldehyde sorption isotherms at 35 and 45°C. The data are reported on an amorphous basis to normalize the sorption data to account for changes in crystallinity developed during the sorption experiments. This penetrant-induced crystallization is discussed in more detail later in this work. Within the uncertainty of the data, the isotherms are essentially convex to the pressure axis over most of the pressure range explored. Typically, sorption isotherms of organic penetrants in glassy polymers at low pressures are concave to the pressure axis when the penetrant uptake is dominated by sorption in the non-equilibrium excess volume of glassy polymers [2,21]. While there are hints of concavity in the isotherms at low pressure, most of the sorption data are taken in a pressure range where sorption in the equilibrium matrix appears to be the dominant contribution to the overall sorption, and any concavity in the isotherms was too weak to be quantified.

At high penetrant activity, sorption isotherms are often convex to the pressure or activity axis for vapor sorption in rubbery [22] and glassy [23] polymers. Such isotherms are often modeled using the Flory–Huggins equation [24]

$$\ln a = \ln \phi + (1 - \phi) + \chi(1 - \phi)^2, \tag{3}$$

where a is vapor phase penetrant activity, ϕ the penetrant volume fraction in the amorphous regions of the polymer, and χ is the polymer–penetrant interaction parameter. For acetaldehyde, the activity is equal to the relative pressure, p/p_{sat}, where p is the penetrant pressure surrounding the film, and p_{sat} is the saturation vapor pressure. The penetrant volume fraction, ϕ is estimated as follows [25]:

$$\phi = \frac{C_a(V_1/22,414)}{1 + C_a(V_1/22,414)}, \tag{4}$$

where V_1 is the saturated liquid penetrant molar volume, which is 55.8 and 56.4 cm^3/mol for acetaldehyde at 35 and 45°C, respectively [26].

The data in Fig. 7 could not be described by Eq. (3) with a constant value of the interaction parameter, χ. The concentration dependence of χ was modeled using the following empirical power series [27]:

$$\chi = \chi_0 + \chi_1(1 - \phi) + \chi_2(1 - \phi)^2. \tag{5}$$

The best fit parameters were $\chi_0 = -70 \pm 2$, $\chi_1 = 143 \pm 2$, $\chi_2 = -71 \pm 2$, at 35°C, and $\chi_0 = -70 \pm 1$, $\chi_1 = 143 \pm 1$, $\chi_2 = -72 \pm 1$ at 45°C. Based on Eq. (5), an average χ value, $\bar{\chi}$, was defined as follows:

$$\bar{\chi} = \frac{1}{\phi_{max}} \int_0^{\phi_{max}} \chi \, d\phi, \tag{6}$$

where ϕ_{max} is the highest penetrant volume fraction measured in the study. The values of $\bar{\chi}$ at 35 and 45°C are 0.97 ± 0.08 and 0.93 ± 0.04, respectively. Within the uncertainty of the parameters, the average χ values are independent of temperature. As a result, the isotherms in Fig. 7 are almost coincident over the entire range of relative pressures explored.

Penetrant solubility in the amorphous regions of the polymer is defined as [13]

$$S_a = \frac{C_a}{p}, \tag{7}$$

where p is the partial pressure of penetrant in the contiguous gas phase. Solubility coefficients typically obey a van't Hoff expression [13,28]:

$$S = S_0 \exp\left[\frac{-\Delta H_S}{RT}\right], \tag{8}$$

where S_0 is a front factor, R the gas constant, and T is absolute temperature. Based on a fit of the sorption data to Eq. (8) as suggested by Miranda et al. [29], the average heat of sorption was -26.3 ± 0.8 kJ/mol. The heat of condensation of pure acetaldehyde at 40°C, the midpoint of the temperature range explored in this study, is -25.7 kJ [26]. Therefore, the enthalpy of sorption, ΔH_S is dominated by the pure acetaldehyde enthalpy of condensation.

3.4. Acetaldehyde-induced crystallization and microvoid formation

Fig. 8 presents an example of Fickian kinetics of acetaldehyde uptake at 45°C. In this experiment, the initial acetaldehyde pressure, p_i, was 20.0 cmHg, and the final acetaldehyde pressure, p_f, was 30.0 cmHg. M_t is the acetaldehyde uptake at time t, and M_∞ is the acetaldehyde uptake at equilibrium. The fractional mass uptake, M_t/M_∞, increases linearly with $t^{1/2}$ at short times, consistent with diffusion-controlled sorption. However, the data in Figs. 8–11 are not used to evaluate diffusion coefficients due to the difficulty caused by the curled sample specimens in estimating the effective surface area available for diffusion.

At 45°C and pressures above 30.0 cmHg, acetaldehyde uptake kinetics displayed characteristics of solvent-induced crystallization [30,31]. As shown in Fig. 9a, the initial uptake kinetics are Fickian (i.e. mass uptake is a linear function of $t^{1/2}$), but beyond approximately 40 $min^{1/2}$ (cf. Fig. 9b), the amount of acetaldehyde sorbed in the polymer

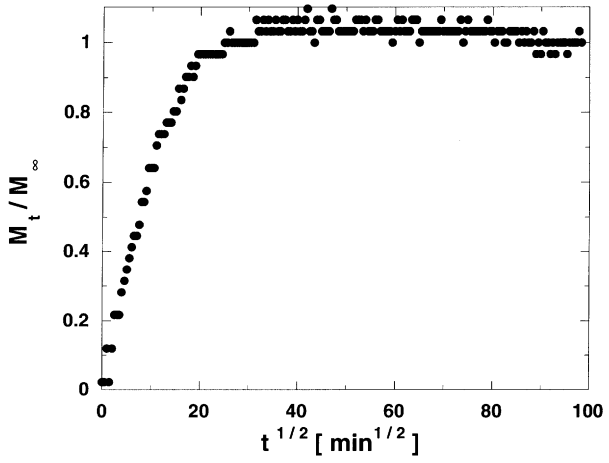

Fig. 8. Kinetics of acetaldehyde sorption in PET at 45°C. $p_i = 20.0$ cm Hg, $p_f = 30.0$ cm Hg, $M_\infty = 0.47 \pm 0.02$ g/100 g.

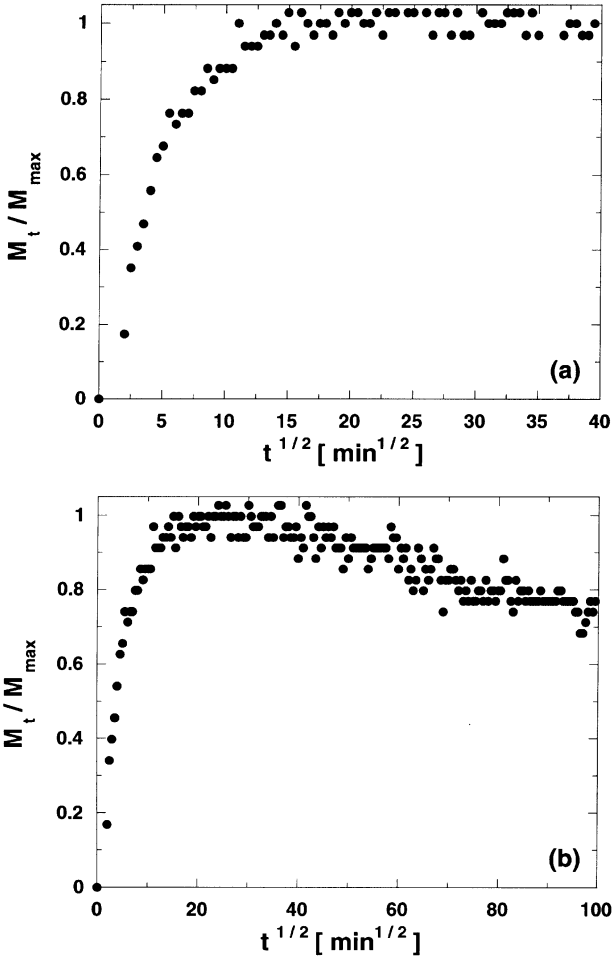

Fig. 9. Acetaldehyde sorption kinetics in PET at 45°C exhibiting low level penetrant-induced crystallization $p_i = 30.0$ cm Hg, $p_f = 40.0$ cm Hg. (a) Uptake profile prior to onset of crystallization, $M_{max} = 0.53 \pm 0.02$ g/100 g; (b) entire uptake profile, $M_\infty = 0.41 \pm 0.02$ g/100 g.

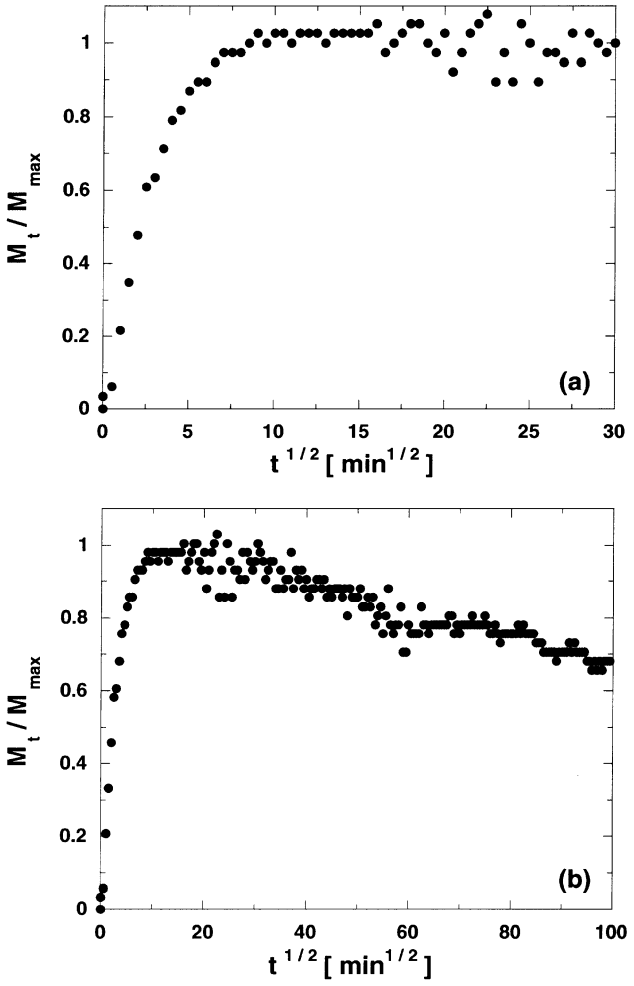

Fig. 10. Acetaldehyde sorption kinetics in PET at 45°C exhibiting moderate penetrant-induced crystallization $p_i = 40.0$ cm Hg, $p_f = 50.0$ cm Hg. (a) Uptake profile prior to onset of crystallization, $M_{max} = 0.61 \pm 0.02$ g/100 g; (b) entire uptake profile, $M_\infty = 0.43 \pm 0.02$ g/100 g.

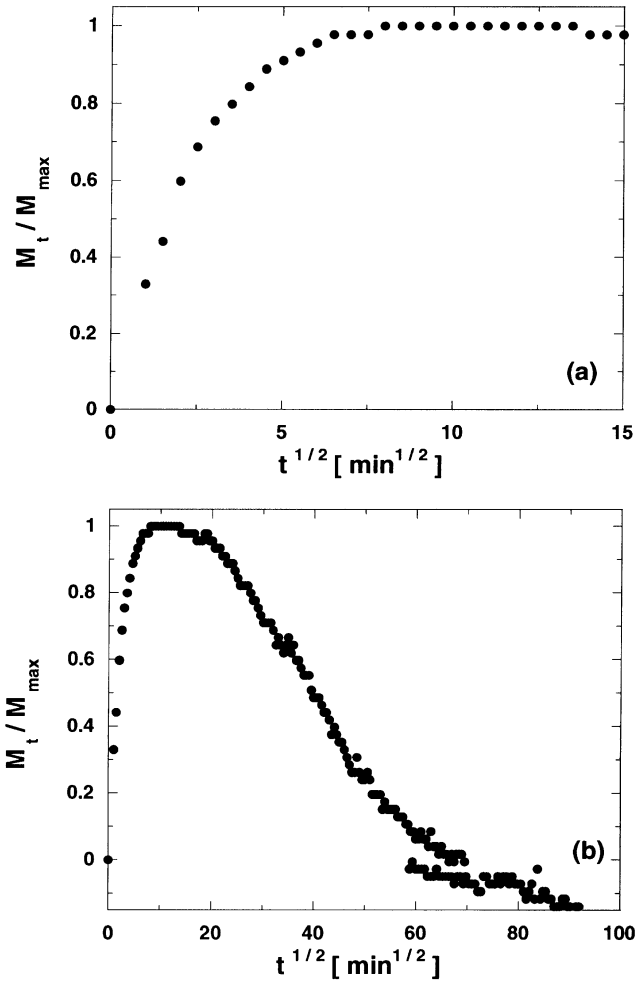

Fig. 11. Acetaldehyde sorption kinetics in PET at 45°C exhibiting strong penetrant-induced crystallization $p_i = 50.0$ cm Hg, $p_f = 60.0$ cm Hg. (a) Uptake profile prior to onset of crystallization, $M_{max} = 0.70 \pm 0.09$ g/100 g; (b) entire uptake profile.

begins to decrease with time. This behavior is a signature of penetrant-induced polymer crystallization and subsequent expulsion of penetrant from the crystalline regions of the sample [30]. In these interval sorption experiments, penetrant induced crystallization was clearly observed at final acetaldehyde pressures of 40, 50, and 60 cmHg at 45°C. The experiments performed at final pressures of 50 cm Hg (Fig. 10a) and 60 cmHg (Fig. 11a) exhibit the same qualitative initial response as that observed in Fig. 9a. The decrease in fractional mass uptake after the initially Fickian response is more pronounced as acetaldehyde pressure increases (cf. Figs. 9b, 10b and 11b). In particular, Fig. 11b shows that all of the incremental acetaldehyde sorption into the sample under these experimental conditions is expelled at long times (~6400 min), presumably due to acetaldehyde-induced crystallization. However, because these are interval kinetic sorption experiments, even at the end of the experiment corresponding to Fig. 11b, there is still a considerable concentration of acetaldehyde remaining in the sample, presumably in the non-crystalline regions of the polymer.

The decrease in penetrant uptake ascribed to penetrant-induced crystallization can be used to estimate the amount of induced crystallization. To a good approximation, penetrant solubility is usually understood to depend on polymer crystalline volume fraction as follows [5,14–18]:

$$S = S_a \Phi_a. \tag{9}$$

Expressed in terms of equilibrium mass uptake, M_∞ (g/100 g polymer), Eq. (9) becomes

$$M_\infty = \frac{100\ \mathrm{MW}}{22414\ \rho_{polymer}} p S_a \Phi_a, \tag{10}$$

where $\rho_{polymer}$ is the polymer density (g/cm^3), MW is the molecular weight of acetaldehyde (44 g/mol), and 22,414 is a conversion factor (cm^3 (STP)/mol). If the penetrant solubility in the amorphous phase is constant, and one assumes that the crystallization occurs after sorption

Table 3
Polymer crystallinity induced by acetaldehyde sorption based on the amount of acetaldehyde expelled from the sample during kinetic sorption experiments (cf. Eq. (11))

p_i (cmHg)	p_f (cmHg)	Wt% (vol.%) crystallinity before experiment	Wt% (vol.%) crystallinity after experiment
30.0	40.0	5.5 (5.0)	12.0 (11.1)
40.0	50.0	12.0 (11.1)	18.9 (17.6)
50.0	60.0	18.9 (17.6)	41.1 (39.3)

equilibrium has essentially been achieved, then Eq. (10) may be written as follows to account for a change in penetrant mass uptake due to a change in crystallinity:

$$M_{max} - M_{\infty} = \frac{100\ MW}{22414\rho_{polymer}} pS_a \Delta\Phi_a, \quad (11)$$

where $\Delta\Phi_a$ is the decrease in amorphous volume fraction due to induced crystallization. The mass of acetaldehyde expelled is the difference between the maximum value of M_t, M_{max}, and the value of M_t at the end of the experiment, M_{∞}. The amount of induced crystallization, $\Delta\Phi_a$, was estimated using Eq. (11). Table 3 presents crystallinity before and after exposure to acetaldehyde at higher pressures. The amount of induced crystallinity increases with increasing pressure. The values shown in Table 3 were used to adjust the three highest pressure data at 45°C in Fig. 7 to an amorphous basis.

Following the acetaldehyde sorption experiments, acetaldehyde was removed from the sample by vacuum desorption. Afterwards, the PET flakes were analyzed by DSC and WAXD. Fig. 12 presents a DSC thermogram of the sample before and after exposure to 60 cmHg acetaldehyde at 45°C. The weight percent crystallinity of both samples was calculated by subtracting the enthalpy of cold crystallization from the enthalpy of melting, and dividing by the heat of fusion of PET (29 cal/g) [12]. The weight percent crystallinity values before and after exposure to the highest activity of acetaldehyde explored in this study are 5.5 wt% (5.0 vol.%) and 36.5 wt% (34.5 vol.%), respectively. The post-acetaldehyde exposure crystallinity value is considered to be in good qualitative agreement with the maximum amount of crystallinity estimated from the amount of penetrant expelled from the polymer during the kinetic sorption experiment (41 wt%). Fig. 13 presents X-ray spectra for the sample before and after exposure to acetaldehyde at 45°C. The post-acetaldehyde sorption sample displays several strong crystalline peaks in addition to the broad amorphous halo. Based on the peak area of the amorphous halo relative to that of the crystalline peaks, the crystallinity level was estimated to be 29 wt% [6]. While this value is lower than that from the DSC and kinetic uptake analyses, this result is consistent with the observation of a significant increase in crystallinity upon exposure to acetaldehyde at 45°C and high activity. Moreover, WAXD will not detect crystals if they are smaller than ~5 nm, whereas sorption and DSC results are sensitive to the total sample crystallinity.

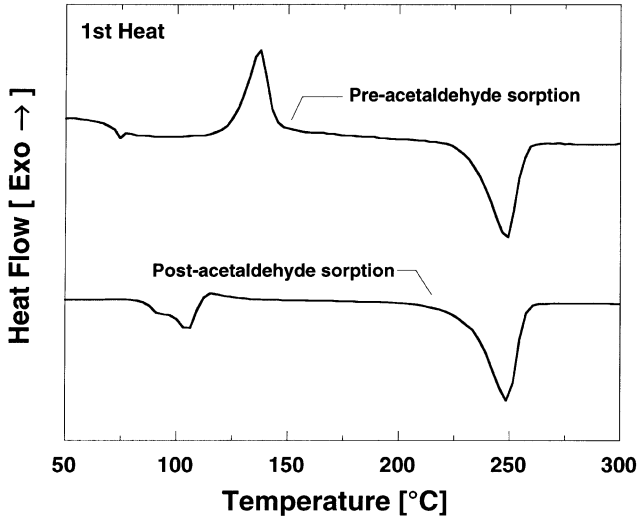

Fig. 12. DSC thermograms of PET before and after exposure to 60 cmHg of acetaldehyde at 45°C.

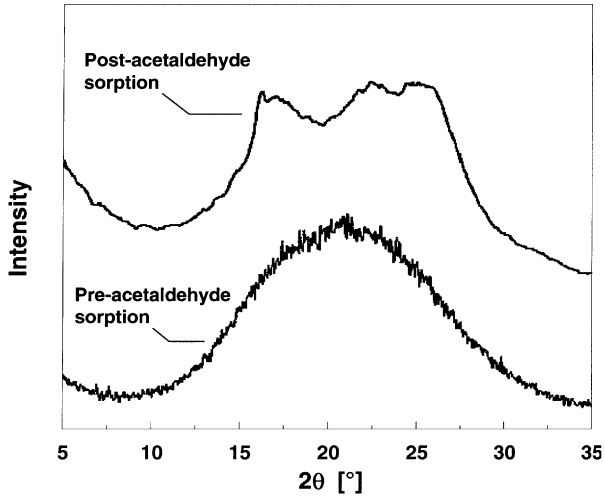

Fig. 13. WAXD spectra of PET before and after exposure to acetaldehyde at 60 cmHg and 45°C.

After exposure to relatively high acetaldehyde pressures and subsequent penetrant-induced crystallization, the sample was exposed to extremely low activity acetaldehyde (i.e. too low to induce structural changes in the polymer) to probe the effect of penetrant-induced crystallization on amorphous solubility. Fig. 14 presents a comparison of the low activity acetaldehyde sorption kinetics in the sample after exposure to high activity acetaldehyde (i.e. the sample kinetic data in Fig. 11) and the sample before exposure to high activity acetaldehyde. After exposure to high activity acetaldehyde vapor, the low activity acetaldehyde uptake is over 300% higher than for a virgin sample. Because crystalline regions of most polymers are understood to preclude penetrant sorption [5,14–18], penetrant solubility typically decreases with increasing crystalline content. Our results,

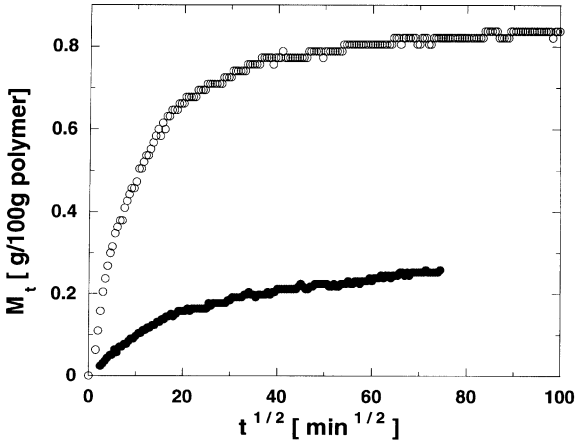

Fig. 14. Low relative pressure acetaldehyde sorption at 35°C in PET before and after exposure to 60 cmHg acetaldehyde at 45°C, $p_i = 0.0$ cmHg, $p_f = 5.0$ cmHg. (●) Before exposure to high activity of acetaldehyde, $M_\infty = 0.25 \pm 0.01$ g/100 g, (○) after exposure to high activity of acetaldehyde, $M_\infty = 0.84 \pm 0.01$ g/100 g.

which are opposite to this trend, suggest that the polymer amorphous phase morphology was altered significantly by exposure to high activity acetaldehyde vapor.

Such a dramatic increase in solubility with increased crystalline content is probably due to the creation of 'microvoids' in the polymer as a by-product of penetrant-induced crystallization. Microvoids, in this context, will be understood to mean regions of the polymer where the local density is lower (or fractional free volume is higher) than it would otherwise be in a sample which had not been exposed to acetaldehyde. The convex acetaldehyde isotherms suggest that the amorphous regions of the polymer are swollen significantly by the penetrant. At 45°C, where solvent-induced crystallization occurs, the crystallites formed may stabilize the swollen polymer structure. Then, when the penetrant is desorbed from the polymer, the swollen polymer structure may form microvoids as a result of kinetic constraints on macromolecular mobility (imposed by the crystals formed during sorption), hindering the volume relaxation of the polymer during penetrant removal. The microvoids would act as high capacity sorption sites in the polymer and would be responsible for the much higher levels of sorption in the sample after exposure to high activity of acetaldehyde. We do not have independent diffraction data to estimate the size scale of these microvoids, so we do not know if the decrease in density is a local scale phenomena (similar to so-called penetrant conditioning effects common in glassy polymers) or occurs on a larger size scale.

While this mechanism of microvoid formation has not been verified independently and must be regarded as speculative, evidence for microvoid formation in PET due to exposure to strongly sorbing penetrants has been presented previously in studies investigating methods to improve the dyeability of PET yarns [32] and in studies investigating the effect of liquid penetrant treatments on the morphology of PET [33–35]. Jameel et al. studied the sorption of liquid dimethylformamide (DMF) in stretched PET films as a function of DMF treatment temperature [33]. PET films were immersed in liquid DMF at temperatures ranging from 21 to 130°C, and equilibrium mass uptake was measured. Mass uptake decreased with increasing temperature and attained a minimum value at approximately 90°C. At higher temperatures, equilibrium DMF uptake increased by 30% as temperature increased to 130°C. This behavior was attributed to the formation of microvoids in the polymer due to rapid crystallization in the penetrant-swollen polymer. The presence of these microvoids was confirmed in further studies by small angle X-ray scattering studies [34].

Weigmann et al. conducted a similar study in which PET fibers were contacted with liquid DMF at temperatures above 100°C [32]. This treatment induced crystallization and microvoid formation. Afterwards, dye uptake was measured [32]. Dye uptake in samples exposed to DMF was four to five times higher than dye uptake in samples that did not experience penetrant-induced crystallization and microvoid formation. Lawton et al. found that contact of PET with organic liquids such as acetone, acetonitrile and acetic acid at 25°C led to microvoid formation, as indicated by abnormally low densities [35]. These composite results support the notion of microvoid formation in PET upon contact with strongly interacting penetrants.

3.5. Correlation of infinite dilution solubility with critical temperature

Penetrant sorption in polymers is regarded as a two step thermodynamic process: (1) condensation of the gaseous penetrant to a liquid-like density and (2) mixing of the pure compressed penetrant with the polymer segments [36]. The first step is governed by penetrant condensability, and the second depends on polymer–penetrant interactions. For penetrants that interact with the polymer matrix primarily via dispersion (i.e. van der Waals) forces, the first step is the dominant contribution to the overall free energy change on sorption, and penetrant solubility scales with measures of penetrant condensability such as penetrant boiling point, critical temperature, or the force constant in the Lennard–Jones potential model [36–38]. In this case, the following relation between penetrant critical temperature and infinite dilution amorphous phase gas solubility at 25°C has been derived using a classical thermodynamics model [37,39,40]:

$$\ln S_a = N + MT_c. \tag{12}$$

In this expression, N is a parameter that depends primarily on polymer–penetrant interactions and polymer free volume. T_c is the penetrant critical temperature, which is widely tabulated for many penetrants of interest [26]. M is constant and has a value of approximately 0.016 K^{-1} for gas dissolution in liquids and in rubbery and glassy polymers [37,41]. While N varies from polymer to polymer, Van

Krevelen recommends average values of −9.7 and −8.7 for rubbery and glassy polymers at 35°C, respectively, when solubility is expressed in cm^3 (STP)/(cm^3·cmHg) [37]. Penetrants with strong dipole or quadrupole moments may be more soluble in a polar polymer matrix, such as PET, than predicted based on Eq. (12) [42,43].

Although Eq. (12) is strictly valid for penetrant sorption in equilibrium matrices, such as liquids or rubbery polymers, it also provides an excellent description of equilibrium solubility in glassy polymers [41]. Over wider ranges of critical temperature, Stern has suggested that penetrant solubility coefficients may be better correlated with the square of reciprocal reduced temperature, $(T_c/T)^2$ [44]

$$\ln S_a = n + m\left(\frac{T_c}{T}\right)^2, \tag{13}$$

where T is the temperature of the experiment, and m and n are the slope and intercept of the correlation line, respectively. This equation may also be derived from fundamental thermodynamic considerations [45].

Fig. 15 presents the solubility of *n*-butane and acetaldehyde (from this study) and other literature penetrant solubility data for PET as a function of both T_c and $(T_c/T)^2$. The solubilities were adjusted to an amorphous basis using Eq. (9) and to infinite dilution conditions when possible. Infinite dilution solubility values were obtained by graphically extrapolating reported solubility values to zero concentration. When it was not possible to extrapolate to infinite dilution, the solubility values were included in Fig. 15, but the conditions of the measurements are noted in the figure caption. Penetrant solubilities increased rather regularly with T_c, in accordance with Eqs. (12) and (13).

The lines in Fig. 15 represents least squares fits of the solubility data for penetrants without significant dipole or quadrupole moments (the penetrants represented by filled symbols in the figures) to Eqs. (12) and (13). The slope in Fig. 15a is 0.019 ± 0.001, which is near the value (0.016) observed for gas dissolution in other liquids and polymers. The intercept, m, is −9.6 ± 0.4, which is in the range of the general values suggested by Van Krevelen. Fig. 15b presents a comparison of the solubility data with Eq. (13). A comparison of the m and n parameter values for PET and several other glassy and rubbery polymers is presented in Table 4. Within the uncertainty of the parameters, the slopes for all of the polymers are the same. The intercept values vary from one polymer to another, and PET has the lowest intercept value, consistent with its lower penetrant solubility values relative to the other polymers.

While there is some scatter of the experimental data around the correlation lines in Fig. 15a and b, a strong correlation of penetrant solubility with critical temperature is noted. As PET is a nonequilibrium glassy polymer whose sorption and transport properties depend on thermal processing history, it is not surprising to observe some scatter in this correlation. Also, the data for several penetrants (methanol, ethyl acetate ($CH_3COOC_2H_5$), and water) are not available at infinite dilution, and penetrant solubility is expected to change with penetrant activity in PET [18]. In addition, the deviation of helium from the correlation lines

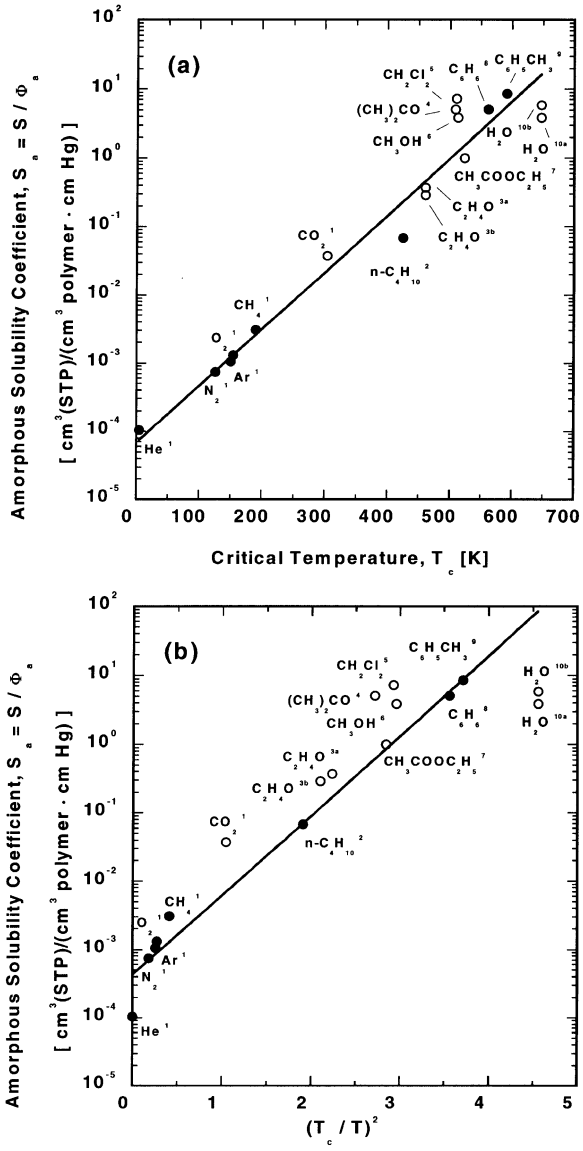

Fig. 15. Correlation of amorphous phase solubility coefficients in PET with (a) critical temperature, T_c and (b) $(T_c/T)^2$. Unless otherwise noted, solubilities are infinite dilution values. The best lines through the data for nonpolar penetrants in these figures yield the following slope and intercept values: (a) slope (M) = − 9.6 ± 0.4 K^{-1}, intercept (N) = 0.019 ± 0.001, correlation coefficient (R^2) = 0.984; (b) slope (m) = − 2.68 ± 0.2, intercept (n) = − 7.8 ± 0.3, correlation coefficient (R^2) = 0.976. (●) non-polar penetrants, (○) polar and quadrupolar penetrants. Key: 1. He, N_2, Ar, O_2, CH_4, CO_2: 25°C, amorphous [18]; 2. *n*-C_4H_{10}: 35°C, 5.0 vol.% crystallinity (this work); 3a. C_2H_4O, 35°C, 5.0 vol.% crystallinity (this work); 3b. 45°C, 5.0 vol.% crystallinity (this work); 4. $(CH_3)_2CO$: 35°C, 38 vol.% crystallinity [2]; 5. CH_2Cl_2: 24°C, 43 vol.% crystallinity [53]; 6. CH_3OH: 25°C, 23 vol.% crystallinity, p/p_{sat} = 1.0 [52]; 7. $CH_3COOC_2H_5$: 30°C, 22 vol.% crystallinity, p/p_{sat} = 0.6[64]; 8. C_6H_6: 25°C, amorphous [65]; 9. $C_6H_5CH_3$: 23°C, 24 vol.% crystallinity [64]; 10a. H_2O: 30°C, 3 vol.% crystallinity [66]; 10b. H_2O: 25°C, ~20 vol.% crystallinity [67].

Table 4
Slope (m) and intercept (n) of correlation of the natural logarithm of infinite dilution penetrant solubility with $(T_c/T)^2$[a]

Material	m	n
Amorphous PET	2.68 ± 0.2	−7.8 ± 0.3
Amorphous polyethylene [22]	2.62	−7.5
PDMS [22]	2.475	−5.9
TFE/BDD87 [70]	2.56 ± 0.07	−5.1 ± 0.14

[a] Solubility units are $cm^3(STP)/(cm^3 \cdot cmHg)$. PDMS is poly(dimethylsiloxane); TFE/BDD87 is a random copolymer prepared from 87 mol% 2,2-bistrifluoromethyl-4,5-difluoro-1,3-dioxole (BDD) and 13 mol% tetrafluoroethylene (TFE).

in Fig. 15 is consistent with a large deviation in helium solubility from a similar correlation for gas sorption in polyethylene [44].

In contrast, the solubility of water is significantly below that anticipated based on its critical temperature. This result may reflect an unfavorable interaction between water and the lipophilic environment of the PET matrix. Also, water undergoes self-association through hydrogen bonding and, based on the results in Fig. 15, these interactions may be more favorable than any PET–water interactions which might otherwise boost water solubility in PET. Similar phenomena have been reported for the dissolution of polar and quadrupolar penetrants in aromatic polyamides. The polar amide linkages in the polymer backbone only undergo solubility-enhancing interactions with polar or quadrupolar penetrants if the amide linkage self-hydrogen bonding is weaker than the potentially favorable interactions between the amide linkages and the penetrant [46]. Carbon dioxide also exhibits substantial positive deviations from the correlation in Fig. 15b, suggesting potential favorable interactions of this quadrupolar penetrant with the polar PET matrix.

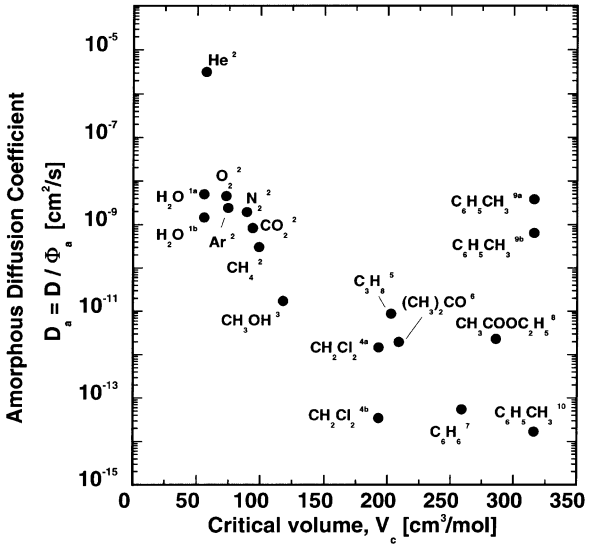

Fig. 16. Effect of penetrant size on diffusion coefficients in PET. Diffusion coefficients corrected to an amorphous basis. Unless otherwise noted below, diffusion coefficients are infinite dilution values. Key: 1a. H_2O: 25°C, ~20 vol.% crystallinity [67]; 1b. H_2O: 30°C, $p/p_{sat} = 0.478$, 3 vol.% crystallinity [66]; 2. He, N_2, Ar, O_2, CH_4, CO_2: 25°C, amorphous [5]; 3. CH_3OH: 25°C, 23 vol.% crystallinity, $p/p_{sat} = 1.0$ [52]; 4a. CH_2Cl_2: 24°C, 43 vol.% crystallinity [53]; 4b. CH_2Cl_2: 21°C, amorphous [55]; 5. C_3H_8: 55°C [68]; 6. $(CH_3)_2CO$: 35°C, 38 vol.% [2]; 7. C_6H_6: 40°C, amorphous [65]; 8. $CH_3COOC_2H_5$: 30°C, 22 vol.% crystallinity, $p/p_{sat} = 0.6$ [64]; 9a. $C_6H_5CH_3$: 34°C, 2.8 vol.% crystallinity, $p/p_{sat} = 1.0$ [69]; 9b. $C_6H_5CH_3$: 34°C, 29 vol.% crystallinity, $p/p_{sat} = 1.0$ [69]; 10. $C_6H_5CH_3$: 23°C, 24 vol.% crystallinity [64].

3.6. Correlation of diffusion coefficients with penetrant size in PET

Penetrant diffusion coefficients generally decrease with increasing penetrant size [47]. A convenient measure of penetrant size is critical volume, which is tabulated for a wide range of penetrants [26]. Fig. 16 presents diffusion coefficients in PET which have been reported in the literature. In this figure, the diffusion coefficients were corrected to account for the effect of crystallinity and were extrapolated to infinite dilution conditions when possible as described in Appendix A. When the data could not be extrapolated to infinite dilution, the penetrant relative pressure at which the diffusion coefficient measurements were performed is indicated in the figure caption. Fig. 16 illustrates the enormous range of diffusion coefficients in PET. As penetrant size increases from He to benzene, diffusion coefficients at infinite dilution decrease by more than eight orders of magnitude. The literature data reported in Fig. 16 were obtained using PET samples with a wide variety of thermal history and processing histories. Some of the scatter of the data in Fig. 16, even after the normalization for crystallinity and, when possible, extrapolation to infinite dilution illustrates the difficulty in comparing diffusion coefficients obtained at different experimental conditions and for samples of different processing histories. Moreover, the wide difference in diffusion coefficients reported for the same penetrant (toluene) at very different penetrant activities (from infinite dilution to saturation), indicates that the diffusion coefficient of such condensable, aromatic penetrants depends strongly on penetrant concentration [48].

To better isolate the influence of penetrant size on diffusion coefficients in PET, Fig. 17 was prepared. In this figure, data were included only if they could be extrapolated to infinite dilution conditions based on experimental data in the original references. The data in Fig. 17 were adjusted to 25°C as described in Appendix A, since this was the temperature at which the largest number of data points were reported in the literature.

These infinite dilution diffusion coefficients for penetrants in amorphous PET exhibit, to a reasonable approximation, a simple power law dependence on penetrant critical volume [49]:

$$D_a = \frac{\tau}{V_C^{\eta}}, \tag{14}$$

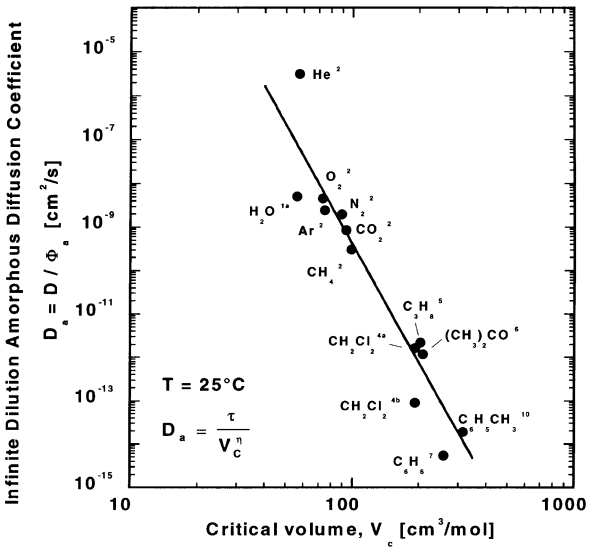

Fig. 17. Effect of penetrant size on diffusion coefficients in PET: Power law correlation. Only diffusion coefficients that could be extrapolated to amorphous basis, infinite dilution, and 25°C are shown. The best fit parameters of Eq. (14) are: $\eta = 9.1 \pm 0.9$, $\tau = 5.66 \pm 1.2 \times 10^8$ cm^2[s(cm^3/mol)^{21}]. The key for the literature data is presented in the caption of Fig. 16.

where τ and η are adjustable constants. While this equation is empirical, it is proposed based on analogy with correlations of diffusion coefficients of small molecules in liquids [26,50,51]. A correlation of diffusion coefficients with penetrant critical volume should only be applicable for penetrants small enough that the entire penetrant molecule participates in the diffusion step. For larger penetrants (e.g. long chain hydrocarbons), diffusion steps may occur via motion of only part of the penetrant molecule, so critical volume would not be expected to capture the effective size of a penetrant unit participating in a diffusion step. In this case, diffusion coefficients should become less sensitive to penetrant size than indicated in this equation. Of course, critical volume cannot capture the influence of penetrant shape on diffusion coefficients, so this correlation is expected to be less accurate for asymmetric penetrants.

The exponent in Eq. (14), η, characterizes the strength of the dependence of diffusion coefficients on penetrant size. Polymers with larger values of η will have more significant changes in diffusivity over a given range of critical volume than polymers with smaller η values. Table 5 provides a list of η values for penetrant diffusion in liquids, rubbery polymers, and glassy polymers. As expected, liquids have the weakest dependence of diffusion coefficients on penetrant size, followed by rubbery polymers, as exemplified by poly(dimethylsiloxane), the most flexible rubbery polymer known. The exponent for the glassy polymers are substantially greater than those of the rubbery polymer and liquids, consistent with the more restricted local segmental mobility of glassy polymers.

Eq. (14) may be used to predict the diffusion coefficients of various molecules of interest, such as various flavor molecules, whose critical volumes are known or may be estimated. For example, the critical volume of d-limonene was estimated to be 497 cm^3/mol using group contribution methods [26]. The critical volume was then used in Eq. (14) to calculate a diffusion coefficient of 2×10^{-16} cm^2/s for *d*-limonene in PET at 25°C.

Table 5
Power law exponents for diffusion coefficients correlated with critical volume

Material	Material type	η
Low molecular mass organic liquids (e.g. hexane, heptane, benzene) [26,50,51]	Liquid	0.45
Poly(dimethyl siloxane) [49]	Rubber	2.2
Polysulfone [49]	Glass	8.4
PET	Glass	9.1 ± 0.9
Poly(vinyl chloride) [49]	Glass	10.5

4. Conclusions

The dual mode sorption model adequately describes *n*-butane sorption in PET. Acetaldehyde equilibrium sorption isotherms at 35 and 45°C can be described by the Flory–Huggins sorption model if the interaction parameter is allowed to vary with concentration. Any acetaldehyde uptake that occurs in the non-equilibrium excess volume associated with the glassy polymer is too low to characterize accurately at the experimental conditions explored. At 45°C and acetaldehyde pressures of 40.0 cmHg and above, acetaldehyde triggers significant crystallization of PET (approximately 37 wt%). Solubility coefficients at low penetrant pressures are markedly higher in the penetrant-crystallized sample than in initially amorphous samples, suggesting the formation of microvoids (which act as highly efficient penetrant sorption sites) in the polymer sample. The logarithm of infinite dilution penetrant solubility in amorphous regions of PET is correlated with penetrant condensability as characterized by T_c, penetrant critical temperature, or by $(T_c/T)^2$, where T is the experiment temperature. Infinite dilution, amorphous phase diffusion coefficients in PET decrease according to a power law relation with increasing penetrant critical volume.

Acknowledgements

The authors gratefully acknowledge the support of Eastman Chemical Company for this research. Mr David Calvert of Eastman Chemical Company provided valuable guidance in the preparation of the microtomed samples. We also thank the Eastman Chemical analytical laboratories for performing much of the sample characterization. Dr T.J. Bastow of CSIRO kindly performed the ^{13}C NMR analysis.

Appendix A.

PET is a glassy polymer that can contain significant levels of crystallinity depending on thermal processing history [52,53]. Crystallites act as impenetrable barriers to penetrant diffusion in polymers [54]. Michaels et al. approximated the influence of crystallinity on diffusivity as follows [5,15,17]:

$$D = \frac{D_a}{\tau\beta}, \tag{A1}$$

where D_a is the amorphous phase diffusion coefficient, τ a geometric impedance factor, and β is a chain immobilization factor. Crystallites force penetrants to follow a tortuous path through amorphous regions. The geometric impedance factor, τ, which is the ratio of the average distance traveled by a penetrant molecule in traversing a sample to the sample thickness, accounts for this effect. Crystallites can also restrict segmental mobility by acting as physical crosslinks. The chain immobilization factor, β, accounts for this effect. Reduction in amorphous phase chain mobility due to the crystallites is generally most pronounced in flexible rubbery polymers. In glassy polymers such as PET, the inherent rigidity of the chain backbone usually imposes more of an impedance to chain mobility than the crystallites, and β is approximately one [5], whereas for rubbery polymers, β is greater than one [15]. The geometric impedance factor, τ, may be a complex function of crystallite amount, shape, size, and orientation [54]. One simple, empirical model describing the impact of crystallinity on impedance factor in PET is [5]:

$$\tau = \frac{1}{\Phi_a}, \tag{A2}$$

where Φ_a is the polymer amorphous volume fraction. With this result, Eq. (A1) is

$$D = D_a\Phi_a. \tag{A3}$$

Based on this simple model, penetrant diffusivity, like solubility, is directly proportional to polymer amorphous volume fraction. Eq. (A3) was used to correct the reported diffusion coefficients for the effect of crystallinity.

The following empirical model of the concentration dependence of diffusivity, often observed for vapor sorption in PET [2,53,55,56], was used to extrapolate the diffusion coefficients to infinite dilution

$$D = D_\infty \exp[\omega C], \tag{A4}$$

where D_∞ is the intercept and ω is the slope of the correlation line when the diffusion coefficients were plotted as a function of concentration.

The extrapolation of diffusion coefficients from the reported temperatures to 25°C relies on the fact that diffusion of small molecules is an activated process and, at temperatures far from thermal transitions in the polymer (e.g. glass transition, melting, etc.), the Arrhenius equation is obeyed [57]:

$$D_a = D_0 \exp\left[\frac{-E_D}{RT}\right] \tag{A5}$$

where D_a is the amorphous phase diffusion coefficient, D_0 is a front factor, E_D is the activation energy for diffusion, R is the gas constant, and T is the absolute temperature. When activation energies of diffusion were reported, the diffusion coefficients were adjusted, when necessary, to 25°C using Eq. (A5).

In some cases, the temperature of the experiments was not 25°C, and the activation energy of diffusion was not reported. In these cases, we estimate the activation energy of diffusion using the known correlation, reported by Barrer [58] and VanAmerongen [59], between the front factor and activation energy:

$$\ln D_0 = a\frac{E_D}{RT} - b, \tag{A6}$$

where a and b are independent of penetrant type. The parameter a is independent of polymer type and has a universal value of 0.64 [60]. b has a value of $-\ln(10^{-4}\ \mathrm{cm^2/s}) = 9.2$ for rubbery polymers and $-\ln(10^{-5}\ \mathrm{cm^2/s}) = 11.5$ for glassy polymers [37]. Eq. (A6) is often referred to as a 'linear free energy' relation. Similar relations between front factors and activation energies are observed for viscosity of organic liquids, molten salts and metals [61] and for first order chemical reaction kinetics [62], which are also activated processes described by the Arrhenius equation. Additionally, PET is known to follow this relation both above and below the glass transition temperature [63]. Combining Eqs. (A5) and (A6) gives

$$D_a = \exp\left[-b - (1-a)\frac{E_D}{RT}\right]. \tag{A7}$$

Based on a single value of the infinite dilution, amorphous diffusion coefficient at one temperature, the activation energy can be estimated from Eq. (A7), and this equation can then be used to estimate the diffusion coefficient at 25°C.

References

[1] Begley TH, Hollifield HC. Food technology, 1993. p. 109.
[2] McDowell CC, Freeman BD, McNeely GW. Polymer 1999;40:3487.
[3] McBain JW, Bakr AM. J Am Chem Soc 1926;48:690.
[4] McDowell CC, Coker DT, Freeman BD. Rev Sci Instr 1998;69:2520.
[5] Michaels AS, Vieth WR, Barrie JA. J Appl Phys 1963;34:13.
[6] McDowell CC, Freeman BD, McNeely GW, Haider MI, Hill AJ. J Polym Sci: Part B: Polym Phys 1998;36:2981.
[7] Puff W. Comput Phys Commun 1983;30:359.
[8] Hill AJ. Positron annihilation lifetime spectroscopy to probe free volume effects in polymers and composites. In: Tant MR, Connell JW, McManus HLN, editors. High temperature properties and applications of polymeric materials. Washington, DC: American Chemical Society, 1995. p. 63.
[9] Fyfe CA. Solid state NMR for chemists. Ontario: CFC Press, 1983. p. 55.

[10] Fischer EW, Fakirov SJ. Mat Sci 1976;11:1041.
[11] Lawton EL, Ringwald EL. Physical constants of poly(oxyethylene-oxytereohthaloyl) (poly(ethylene terephthalate)). In: Brandup J, Immergut EH, editors. Polymer handbook, V/101. New York: Wiley, 1989.
[12] Roberts RC. Polymer 1969;10:115.
[13] Ghosal K, Freeman BD. Polym Adv Tech 1994;5:673.
[14] Myers AW, Rogers CE, Stannett V, Swarc M. Modern plastics 1957;34:157.
[15] Michaels AS, Parker Jr, R B. J Polym Sci 1959;16:53.
[16] Michaels AS, Bixler HJ. J Polym Sci 1961;50:393.
[17] Michaels AS, Bixler HJ. J Polym Sci 1961;50:413.
[18] Michaels AS, Vieth WR, Barrie JA. J Appl Phys 1963;34:1.
[19] Paul DR. Ber Bunsenges Phys Chem 1979;83:294.
[20] Serad GE. MS. Dissertation, North Carolina State University, 1999.
[21] McDowell CC, Freeman BD, McNeely GW. J Polym Sci: Part B: Polym Phys 1999;37(21):2973.
[22] Suwandi MS, Stern SA. J Polym Sci 1973;11:663.
[23] Berens AR. J Appl Polym Sci 1989;37:901.
[24] Flory PJ. J Chem Phys 1950;18:108.
[25] Singh A, Freeman BD, Pinnau I. J Polym Sci Part B: Polym Phys 1998;36:289.
[26] Reid RC, Prausnitz JM, Poling BE. The properties of gas and liquids, 4th ed. New York: McGraw-Hill, 1987. p. 741.
[27] Gundert F, Wolf BA. Polymer–solvent interaction parameters. In: Brandrup J, Immergut EH, editors. Polymer handbook. New York: Wiley, 1989. p. VII/173.
[28] Naylor T. Permeation properties. In: Allen G, editor. Comprehensive polymer science: the synthesis, characterization, reactions, and applications. New York: Pergamon Press, 1989. p. 643.
[29] Miranda NR, Freeman BD, Hopfenberg HB. J Memb Sci 1991;60:147.
[30] Overburgh N, Berghmans H, Smets G. Polymer 1975;16:703.
[31] Ware R, Tirtowidjojo S, Cohen C. J Appl Polym Sci 1981;26:2975.
[32] Weigmann H-D, Scott MG, Ribnick AS, Rebenfeld L. Textile Res J 1976;46:574.
[33] Jameel H, Waldman J, Rebenfeld L. J Appl Polym Sci 1981;26:1795.
[34] Jameel H, Noether HD, Rebenfeld L. J Appl Polym Sci 1982;27:773.
[35] Lawton EL, Cates DM. Textile Res J 1978;48:478.
[36] Petropoulos JH. Mechanisms and theories for sorption and diffusion of gases in polymers. In: Paul DR, Yampol'skii YP, editors. Polymeric gas separation membranes. Boca Raton: CRC Press, 1994. p. 17.
[37] VanKrevelen D. Properties of polymers: their correlation with chemical structure, their numerical estimation and periction from additive group contributions. Amsterdam: Elsevier, 1990. p. 875.
[38] Stannett VT. Simple gases. In: Crank J, Park GS, editors. Diffusion in polymers, New York: Academic Press, 1968. p. 41.
[39] Gee G. Quart Revs 1947;1:265.
[40] Barrer RM, Skirrow GJ. J Appl Polym Sci 1948;3:564.
[41] Toi K, Morel G, Paul DR. J Appl Polym Sci 1982;27:2997.
[42] Ghosal K, Chern RT, Freeman BD, Daly WH, Negulesco II M. Macromolecules 1996;29:4360.
[43] Bondar VI, Freeman BD, Pinnau I. J Polym Sci, Polym Phys Ed 1999;37:2463.
[44] Stern SA, Mullhaupt JT, Gareis PJ. AIChE J 1969;15:64.
[45] Bondar VI, Freeman BD, Yampol'skii YP. Macromolecules 1999;32:6173.
[46] Morisato A, Ghosal K, Freeman BD, Chern RT, Alvarez JC, delaCampa JGE, Lozano AE, deAbajo J. J Memb Sci 1995;104:231.
[47] Crank J, Park GS. In: Crank J, Park GS, editors. Diffusion in polymers. Oxford: Oxford Science Publications, 1968. p. 1.
[48] Sadler G, Pierce D, Lawson A, Suvannunt D, Senthil V. Food additives and contaminants 1996;13:979.
[49] Freeman BD, Pinnau I. Membrane materials design considerations for gas separations. In: Freeman BD, Pinnau I, editors. Polymeric membranes for gas separations: chemistry and materials science. Washington, DC: American Chemical Society, 1999. p. 1.
[50] Tyn MT, Calus WF. Processing 1975;21:16.
[51] Tyn MT, Calus WF. J Chem Eng Data 1975;20:106.
[52] Billovits GF. Polymer 1988;29:1468.
[53] Liu C-P, Neogi P. J Macromol Sci-Phys 1992;B31:265.
[54] Weinkauf DH, Paul DR. Effects of structural order on barrier properties. In: Koros WJ, editor. Barrier polymers and structures. Washington, DC: American Chemical Society, 1990. p. 60.
[55] Liu C-P, Neogi P. J Appl Polym Sci 1988;35:21.
[56] Fujita H. Organic vapors above the glass transition temperature. In: Crank J, Park GS, editors. Diffusion in polymers. New York: Academic Press, 1968. p. 75.
[57] Barrer RM. Trans Faraday Soc 1939;35:644.
[58] Barrer RM. Trans Faraday Soc 1942;38:322.
[59] VanAmerongen GJ. J Appl Phys 1946;17:972.
[60] Barrer RM, Skirrow G. J Polym Sci 1948;3:549.
[61] Barrer RM. Trans Faraday Soc 1943;39:48.
[62] Leffler JE. J Org Chem 1955;20:1202.
[63] Koros WJ. In: Koros WJ, editor. Barrier polymers and structures, Washington, DC: American Chemical Society, 1990. p. 60.
[64] Hernandez RJ, Giacin JR, Shirakura A, Jayaraman K. Diffusion and sorption of organic vapors through oriented poly(ethylene terephthalate) films of varying thermomechanical history. Proc ANTEC 1990:557.
[65] Patton CJ, Felder RM, Koros WJ. J Appl Polym Sci 1984;29:1095.
[66] Fukuda M, Kawai H. Polymer 1990;31:295.
[67] Yasuda H, Stannett V. J Polym Sci 1962;57:907.
[68] Chen SP. Polym Prepr 1974;15:77.
[69] Nir MM, Ram A. Polym Engng Sci 1996;36:862.
[70] Merkel TC, Bondar V, Nagai K, Freeman BD, Yampolskii Yu P. Macromolecules 1999;32(25):8427.